Peri-implant tissue response and biodegradation performance of a Mg–1.0Ca–0.5Sr alloy in rat tibia

Berglund, Ida S ; Jacobs, Brittany Y ; Allen, Kyle D ; Kim, Stanley E ; Pozzi, Antonio ; Allen, Josephine B ; Manuel, Michele V

Abstract: Biodegradable magnesium (Mg) alloys combine the advantages of traditional metallic implants and biodegradable polymers, having high strength, low density, and a stiffness ideal for bone fracture fixation. A recently developed Mg–Ca–Sr alloy potentially possesses advantageous characteristics over other Mg alloys, such as slower degradation rates and minimal toxicity. In this study, the biocompatibility of this Mg–Ca–Sr alloy was investigated in a rat pin-placement model. Cylindrical pins were inserted in the proximal tibial metaphyses in pre-drilled holes orthogonal to the tibial axis. Implant and bone morphologies were investigated using CT at 1, 3, and 6 weeks after implant placement. At the same time points, the surrounding tissue was evaluated using HE, TRAP and Goldner's trichrome staining. Although gas bubbles were observed around the degrading implant at early time points, the bone remained intact with no evidence of microfracture. Principle findings also include new bone formation in the area of the implant, suggesting that the alloy is a promising candidate for biodegradable orthopedic implants.

DOI: https://doi.org/10.1016/j.msec.2015.12.002

Materials Science and Engineering C 62 (2016) 79–85

Contents lists available at ScienceDirect

Materials Science and Engineering C

journal homepage: www.elsevier.com/locate/msec

Peri-implant tissue response and biodegradation performance of a Mg–1.0Ca–0.5Sr alloy in rat tibia☆

Ida S. Berglund [a], Brittany Y. Jacobs [b], Kyle D. Allen [b], Stanley E. Kim [c], Antonio Pozzi [c,d], Josephine B. Allen [a], Michele V. Manuel [a,*]

[a] Department of Materials Science and Engineering, University of Florida, Gainesville, FL 32611, USA
[b] Department of Biomedical Engineering, University of Florida, Gainesville, FL 32610, USA
[c] Department of Small Animal Clinical Sciences, Gainesville, FL 32610, USA
[d] Clinic of Small Animal Surgery, University of Zurich, Switzerland

ARTICLE INFO

Article history:
Received 2 March 2015
Received in revised form 13 November 2015
Accepted 2 December 2015
Available online 3 December 2015

Keywords:
Magnesium
Calcium
Strontium
Biodegradable alloy
Rat preclinical model

ABSTRACT

Biodegradable magnesium (Mg) alloys combine the advantages of traditional metallic implants and biodegradable polymers, having high strength, low density, and a stiffness ideal for bone fracture fixation. A recently developed Mg–Ca–Sr alloy potentially possesses advantageous characteristics over other Mg alloys, such as slower degradation rates and minimal toxicity. In this study, the biocompatibility of this Mg–Ca–Sr alloy was investigated in a rat pin-placement model. Cylindrical pins were inserted in the proximal tibial metaphyses in pre-drilled holes orthogonal to the tibial axis. Implant and bone morphologies were investigated using μCT at 1, 3, and 6 weeks after implant placement. At the same time points, the surrounding tissue was evaluated using H&E, TRAP and Goldner's trichrome staining. Although gas bubbles were observed around the degrading implant at early time points, the bone remained intact with no evidence of microfracture. Principle findings also include new bone formation in the area of the implant, suggesting that the alloy is a promising candidate for biodegradable orthopedic implants.

1. Introduction

Research on biodegradable magnesium (Mg) alloys is steadily increasing due to their potential to replace currently used fracture fixation devices [1]. Degradable implants eliminate the need for removal surgeries, which are often required for permanent metallic implants such as titanium, stainless steels, and cobalt–chromium alloys [2,3]. Metallic implants can also corrode or release toxic wear products, leading to hostile local or systemic reactions [2,4]. Although biodegradable polymers, such as poly-lactic acid (PLA) or poly-glycolic acid (PGA), are frequently used clinically, these materials are limited in their applications by their relatively low strength compared to traditional metallic implants [5]. Polymeric devices may leave polymeric debris, which can lead to local inflammatory responses and implant loosening [5–8]. Another unfortunate consequence of the use of these polymeric materials, especially those based on PLA, is the long degradation time resulting in foreign-body reactions after implantation [5,8,9]. Magnesium, on the other hand, degrades rapidly, has a low density, and is generally considered biocompatible. Moreover, Mg has stiffness similar to that of bone, potentially reducing the risk of stress shielding effects that can occur with traditional metallic implants [2,10,11]. Mg also has high strength relative to polymeric materials and could thereby support load bearing structures, potentially making it ideal for resorbable implants placed into bone. However, controlling the degradation rate of Mg remains a challenge. This is crucial in implant applications since hydrogen gas evolved during degradation can compromise the mechanical support required for fracture healing processes, while rapid degradation also affects the mechanical integrity of the implant. Although surface treatments and coatings can slow the initial rate of degradation, these processes are often complicated and expensive [12], making alloying a more practical option. Among various systems previously studied, Mg–Ca alloys have shown attractive responses, including improved degradation behavior and biocompatibility [13–15]. Recently, our research group and others have been exploring the potential to create implants based on Mg–Ca–Sr [16,17]. Mg–Ca–Sr alloys have shown reduced degradation rates compared to cast binary Mg–Ca and Mg–Sr alloys with similar alloying amount [13,18]. In addition, Sr may assist in the bone healing process. Administration of Sr, either as a

☆ Author contributions: Kim, Pozzi, K. Allen, J. Allen, and Manuel designed the experiments; Berglund, Jacobs, Kim, Pozzi, and K. Allen collected the data; Berglund, Kim, Pozzi, K. Allen, J. Allen, and Manuel contributed in data analysis and interpretation; Berglund prepared the manuscript; Berglund, K. Allen, J. Allen, Pozzi, Kim and Manuel discussed the results and implications, and critically analyzed, modified and commented on the manuscript during all stages. All authors have read and approved the final submitted manuscript.

* Corresponding author.
E-mail address: mmanuel@mse.ufl.edu (M.V. Manuel).

http://dx.doi.org/10.1016/j.msec.2015.12.002

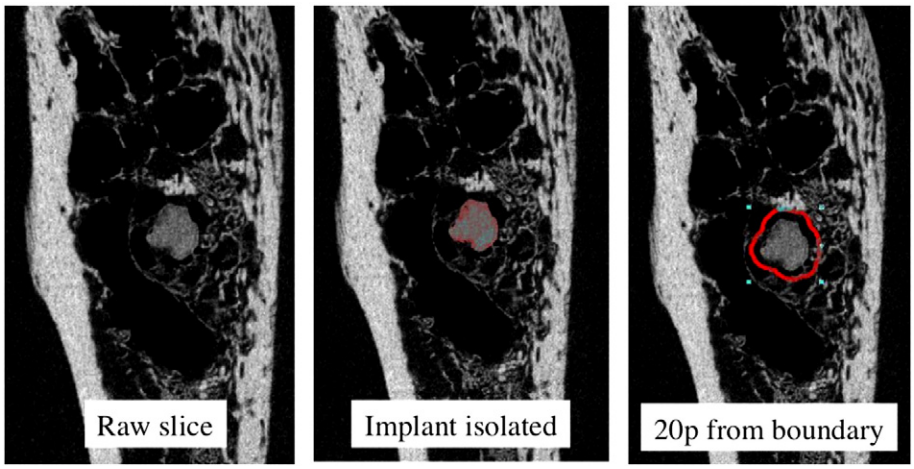

Fig. 1. μCT images showing how pixel distances from the implant boundary are determined, as used in BIC measurements.

dietary supplement in the form of salts [19–21] or when incorporated into implant material [22–24], has shown to promote osteoblast proliferation and improve osseointegration. While preliminary *in vitro* testing on this ternary Mg–Ca–Sr alloy has confirmed reduced degradation rates compared to binary alloys, and non-cytotoxic responses in osteoblastic cell cultures [16], the *in vivo* response is unknown. Understanding the biodegradation performance of Mg-Ca-Sr alloys and their effect on surrounding tissue is crucial for future design and optimization. The objective of the current study is to assess the local tissue response when Mg–1.0 wt.%Ca–0.5 wt.%Sr alloy is implanted into the rat tibia.

2. Materials and methods

2.1. Alloy preparation

Cylindrical Mg–1.0 wt.%Ca–0.5 wt.%Sr alloy pins machined from as-cast material were used as implants [16]. Cast samples were cut using a low-speed diamond saw, followed by machining down to a 0.8 mm diameter smooth surface using a lathe. The cutting and machining processes were performed using oil-based lubricants. Alloy pins were cleaned in soap and ethanol and sterilized in an ethylene oxide gas chamber prior to implantation.

2.2. Experimental design

24 adult male Sprague–Dawley rats with a body weight of 250–300 g were randomly divided into five groups: Mg pin at 1 week (n = 4), Mg pin at 3 weeks (n = 4), Mg pin at 6 weeks (n = 6), poly-L-lactic (PLLA) pin at 6 weeks (n = 6), and naïve healthy controls (n = 4). Because PLLA and Mg were only compared at the final time point, a higher sample number at 6 weeks was used to provide a more robust estimate of the mean and standard deviation of both groups. Cylindrical Mg alloy pins had a diameter of 0.8 mm (as described above). Biodegradable PLLA pins with a diameter of 1.1 mm were obtained commercially (SmartPin®, Conmed Linvatec, Largo, FL) and used for qualitative comparison. All animal work was approved by the University of Florida Institutional Animal Care and Use Committee and conforms to the AAALAC and NIH ethical guidelines for animal research. In accordance with IACUC-approved humane endpoints, one rat in the PLLA pin group was humanely euthanized due to unanticipated complications during surgery; these complications were unrelated to the pin. One sample from the Mg-1w group was excluded from μCT analysis and quantitative histological evaluation due to inadequate placement discovered during post-processing. One pin in the Mg-1w group was found to be fractured upon dissection, but the sample was included in the analyses as the time of fracture was not known (placement, post-placement, *vs* dissection).

2.3. Surgical procedure

Rats were anesthetized in an isoflurane sleep box (2–5%), then transferred to a sterile field with isoflurane maintained at 1–2% *via* mask inhalation. A medial approach to the proximal tibia was made using a combination of sharp and blunt dissection. A transverse pilot

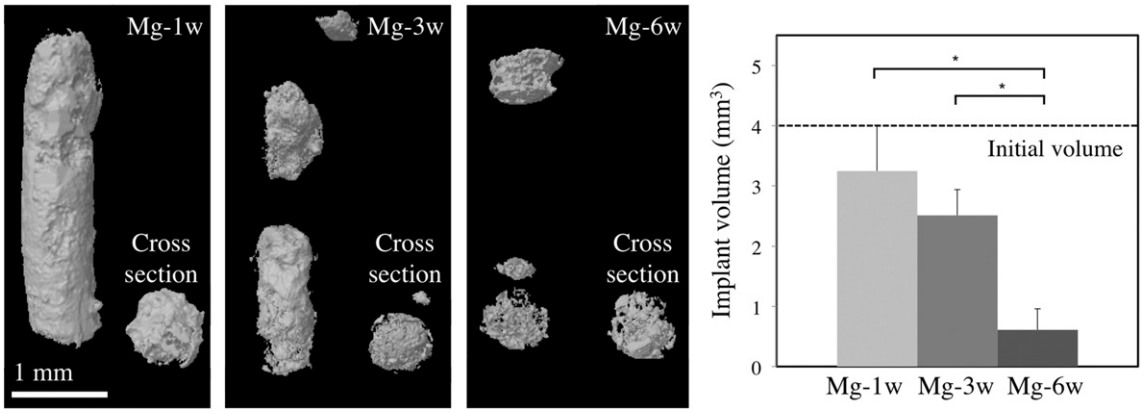

Fig. 2. Representative 3D reconstructions of the implant morphology and the calculated implant volume at different time points. The dashed line in the graph denotes the initial pin volume. The 6w implant volume is significantly smaller compared to 1w (p = 0.028) and 3w (p = 0.014), as indicated by *.

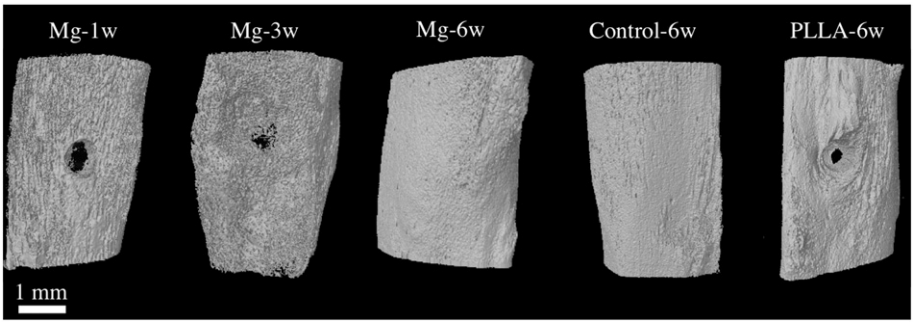

Fig. 3. Representative 3D reconstructions showing the bone morphology around alloy implants at different time points. A 6w control and PLLA-6w are shown for comparison.

hole was made using a 0.8 mm diameter Kirschner wire from medial to lateral in the proximal tibial metaphysis medial to the tibial tuberosity. The biodegradable pin was placed by hand into the pilot hole using a small Jacobs Chuck. Following insertion, the pin was cut at the tibial cortical surface. The subcutaneous layer was closed with 5-0 PDS, and the skin was closed with skin wound clips; wound clips were removed at 14 days post-operation. Buprenorphine was provided intra-operatively and twice a day for 48 h to manage post-operative pain. The animals were allowed to move freely in their cages post-operation and were monitored daily for body-condition score [25], signs of edema at the surgical site, and a visual assessment of animal mobility. No adverse events were noted. At the predefined time points listed above, animals were humanely euthanized; then, soft tissue was carefully dissected and bone was fixed in neutral buffered 10% formalin solution for 48 h, transferred to gauze soaked with phosphate buffered saline, and frozen at −20 °C.

2.4. μCT analyses

The disarticulated tibia was placed in a vial and immersed in saline. Samples were scanned using a Skyscan 1172 μCT system (Bruker Corporation, Billerica, MA) at its maximum resolution of 10.05 μm voxel size. The system was operated using the following settings: 60 kV, 133 μA, 0.7° rotation step, 4 frame average, 2240 × 2240 CCD and 700 ms exposure. Scan time was 20 min per sample. For implant morphology and bone intersection surface measurements, the trans-axial plane of the implant was analyzed. A user-determined implant boundary was created because gray-scale value similarities between the implant and surrounding tissue limited an automated approach. The fraction of bone in the vicinity of the degrading implant was measured. The approach was similar to the bone implant contact (BIC) method commonly used for permanent implant to determine osseointegration by measuring the bone intersection surface area at the implant boundary. Due to the nature of the degrading implant, the bone intersection surface area was instead analyzed at 12, 20 and 28 pixels from the receding implant boundary. A schematic of these distances are shown in Fig. 1. Bone morphology and mineral density were analyzed in the trans-axial plane of the tibia. The volume of interest (VOI) was 8 mm long and centered on the implant. Due to irregular callus formation, two different thresholds were used, one for the high-density cortical bone and a lower threshold for the lower density bone forming as part of the fracture healing process. Bone density measurement was performed on all samples that received alloy pins, and on controls, by analyzing the entire tissue area (excluding voids). Two hydroxyapatite (HA) phantoms with known density (0.25 and 0.75 gHA/cm^3) and similar diameter to the rat tibias were used to convert linear attenuation coefficient to tissue mineral density. One sample from the Mg-1w group was excluded from mineral density measurements as the VOI extended too far proximally.

2.5. Histochemical staining

Calcified sections were prepared by mounting in methyl methacrylate (MMA, Sigma-Aldrich, St. Louis, MO) and cutting along the longitudinal axis of the implant using a rotary microtome with a tungsten carbide knife (4 μm thick sections). The remainders of alloy pins were removed as part of this process. Sections from each tibia were stained with hematoxylin and eosin (H&E) and Goldner's trichrome to study cellularity and mineralization, respectively. Tartrate-resistant acid phosphatase (TRAP) staining was conducted to study bone remodeling. Histologic staining was carried out using standard procedures, with samples qualitatively evaluated using light microscopy (Nikon Eclipse TE2000-U, Nikon Instruments Inc., Melville, NY). The level of TRAP-positive osteoclasts was determined using a computer-assisted histomorphometry approach (MATLAB R2012b, The MathWorks Inc., Natick, MA). An area percentage was determined in each sample by counting red-positive pixels in a radius of approximately 2 mm centered on the implant. For each sample, a minimum of five images (10× magnification) were analyzed from each quadrant around the pin center.

2.6. Statistics

Statistical analyses were performed using one-way analysis of variance (ANOVA) with Mann–Whitney post-hoc tests ($\alpha = 0.05$, Minitab 15, Minitab Inc., State College, PA). A non-parametric method was chosen since the raw data appeared skewed. Mean ± 1 standard deviation is shown in all figures unless otherwise specified.

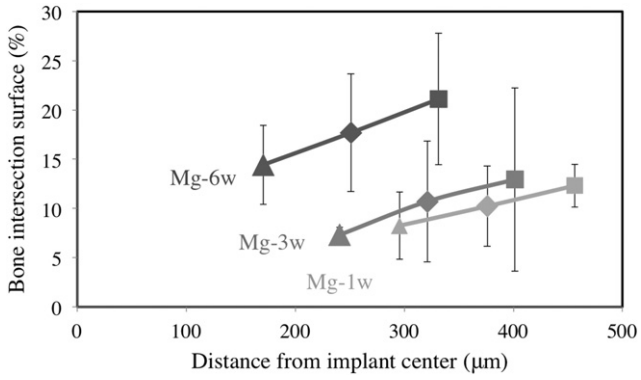

Fig. 4. BIC area presented as the percentage of bone intersection surface at different distances from the alloy implant boundary at different time points. Statistically, there is no significant difference within any of the time point groups at the different pixel distances, or within any of the pixel groups at the different time points.

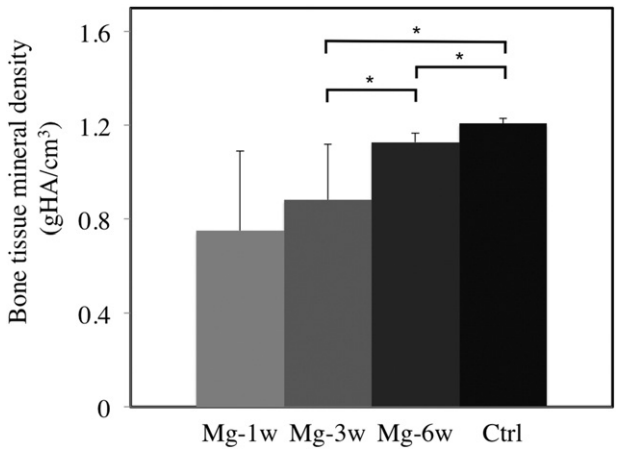

Fig. 5. Average bone mineral density of the tissue in samples with alloy pins at different time points (VOI 8 mm long, centered on the implant). Significant differences are indicated by *. The 3w mineral density value is significantly smaller compared to 6w ($p = 0.0142$) and control ($p = 0.0304$), and the 6w value is smaller compared to control ($p = 0.0252$).

3. Results

3.1. Initial biological response

All rats tolerated the implants well with only mild wound swelling from surgery (<4 days) and no visible evidence of infection. No incidences of limb disuse or lameness were noted in any group.

3.2. Degradation performance

Fig. 2 shows representative 3D reconstructions of the alloy pin at 1w, 3w, and 6w, respectively, along with the calculated average implant volume. 2D area measurements and calculations of implant cross-sectional area were also performed to complement the 3D calculations since inherent VOI errors exist with 3D reconstructions. The implant was almost completely degraded at 6w with less than 10% of the original volume present, which is in accordance with the 2D calculations (not shown). The remaining implant was located in, or adjacent to, the cortical bone. Within the trabecular region, the implant appeared to degrade uniformly. The PLLA pin was intact and did not resorb during the study period.

3.3. Bone morphology

Fig. 3 shows representative μCT 3D reconstructions of the bone surrounding the implants at the different time points. Note that the PLLA pin region appears smaller due to radiolucency of the implant and thus an artifact of the imaging technique. As the alloy degraded, it was consistently replaced by bone by the 6 w time point. To verify new bone was replacing the degrading alloy implant, BIC measurements were performed by calculating the bone area fraction at radial surfaces from the implant boundary at each time point (Fig. 4). No BIC calculations were performed around PLLA pins due to its radiolucency and no BIC information can be provided for the control sample, as the there is no reference point (implant boundary) present from where to make calculations. The average alloy implant radius at the different time points were 0.40 mm (0w), 0.17 ± 0.21 mm (1w), 0.12 ± 0.11 mm (3w) and 0.05 ± 0.02 mm (6w), respectively. For each sample, BIC increased with increasing distance from the implant. BIC measurements also show no decrease in bone area in the proximity of the degrading implants with time. As a reference point, the bone volume per total tissue volume (BV/TV) in the region of interest in the control samples is 90.7 ± 2.2%. No decrease in bone area at fixed distances from the decreasing implant radius suggests that the bone fraction is increasing with time. Complementary, bone density measurements showed mineral density increased with time, as depicted in Fig. 5.

3.4. Tissue response

3.4.1. Hydrogen gas formation

Histological indication of the gas resulting from the degradation process of the alloys, as represented by voids, and the associated tissue

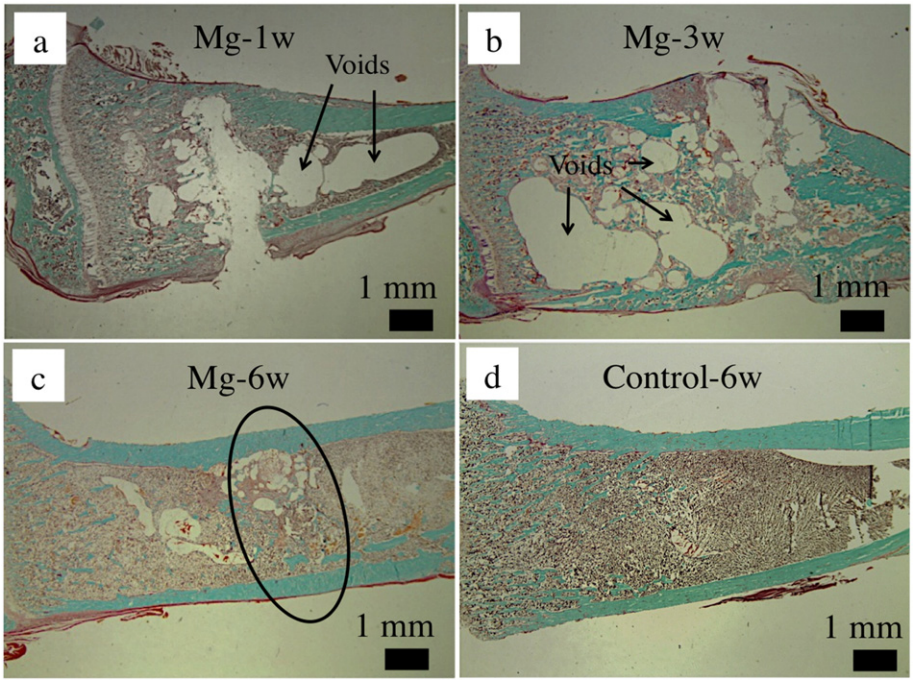

Fig. 6. Representative sections of rat tibia stained with Goldner's trichrome, at 1w (a), 3w (b) and 6w (c) post-surgery, and a 6w control (d), displaying possible gas accumulation in the tissue surrounding the alloy implant, as shown by voids. Mineralized bone at the implantation site can be seen 6w post-surgery (c, circled).

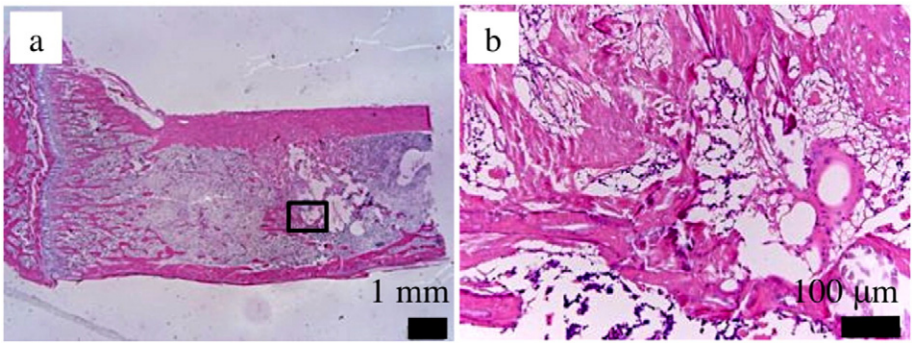

Fig. 7. H&E stained Mg-6w sample showing bone resident cell infiltration at the implantation site at low magnification (a, 1×) and higher magnification (b, 20×). b) is a magnified image from the area inside of the box highlighted in a).

response were seen at the 1w and 3w time points (Fig. 6). However, voids were not observed at 6w, suggesting degradation is slower or complete and gas was systemically absorbed. Despite gas accumulating in the intramedullary cavity at early time points, no evidence of microfracture in the bone was found in either μCT images or histological staining.

3.4.2. Histology

Overall, mild inflammatory response was noted. The 6w samples showed normal morphology with cell proliferation and infiltration into the implant site (Fig. 7). Some fibroblast-like cells were observed adjacent to the implant in all groups; however, a continuous fibrous capsule with thickness of 50–100 μm and with a dense population of fibroblast-like cells was observed around PLLA implants, indicative of a foreign body response (Fig. 8). A fibrous capsule was not observed at any time point in the Mg alloy groups.

At all time points, bone remodeling was observed, as suggested by the osteoblasts (blue/black) and osteoid (red) areas in Fig. 6 (Goldner's stain), and the red-colored osteoclasts in Fig. 9 (TRAP stain). Mineralized bone is shown in Fig. 6, as represented by blue–green color, and newly non-mineralized areas, as represented by red. After 6w, the cortical area at the implantation site was mineralized, showing minimal remnant implant and smooth remodeling of cortical bone (Fig. 6). This was observed in all Mg-6w samples, although to different extents. Earlier time points had varied amounts of mineralization in the cortical area. At all time points, scattered bone tissue formations were seen in the medullary cavity.

3.4.3. Osteoclast quantification

The average level of osteoclasts for each group is shown in Table 1. The calculations were performed on micrographs similar to the ones seen in Fig. 9. No significant difference between different quadrants were detected, but overall, larger amount of osteoclasts were observed at the earlier time points (Mg-1w and Mg-3w) and in the PLLA samples, with the largest amount seen in the Mg implant samples after 3w. Osteoclasts were primarily located in the cortical region and around tissue cavities. The amount of osteoclasts was significantly reduced at the 6w time point, suggesting the degrading implant was well tolerated by the local tissue.

4. Discussion

Biodegradable Mg alloys attempt to combine the advantages of traditional metallic implants and biodegradable polymers. Mitigating gas production by slowing the degradation rate is one of the objectives of alloying. While it is critical to prevent patient discomfort and maintain implant stability, a potentially fatal effect of rapid degradation can occur if, for example, gas bubbles were to reach the vascular system. In the development process of these materials, *in vivo* studies provide crucial information on alloy degradation behavior and biocompatibility. In this study, histological evidence suggests gas formation in the early stages of alloy degradation, which correlates to the decrease in implant volume. More rapid alloy degradation at the early stages is potentially explained by an increased amount of fluid in the cancellous tissue from pin insertion as a result of tissue trauma or fluid accumulation. Faster alloy degradation in the marrow can be attributed to greater vascularization of the cancellous bone, as has been observed and discussed by other researchers [26–28]. A richer blood supply could remove degradation products and neutralize the pH more rapidly, which increases the degradation rate since an alkaline environment promotes a protective hydroxide layer that retards further degradation [29,30]. The gas composition was not measured, but according to the electrochemical reaction $Mg + 2H_2O \rightarrow Mg(OH)_2 + H_2$, the Mg-based pins degrade by giving off hydrogen gas. The hydrogen is then exchanged with the

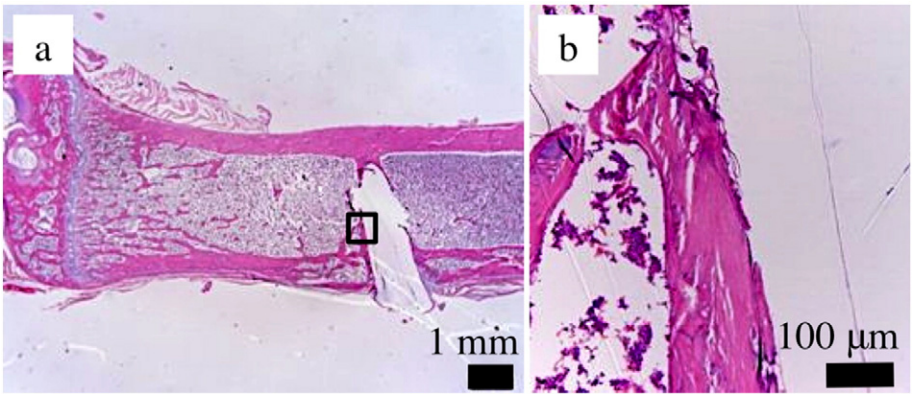

Fig. 8. H&E stained PLLA sample (6 w) showing the encapsulated implant (a, 1×) with a magnification of the fibrous layer (b, 20×). b) is a magnified image from the area inside of the box highlighted in a).

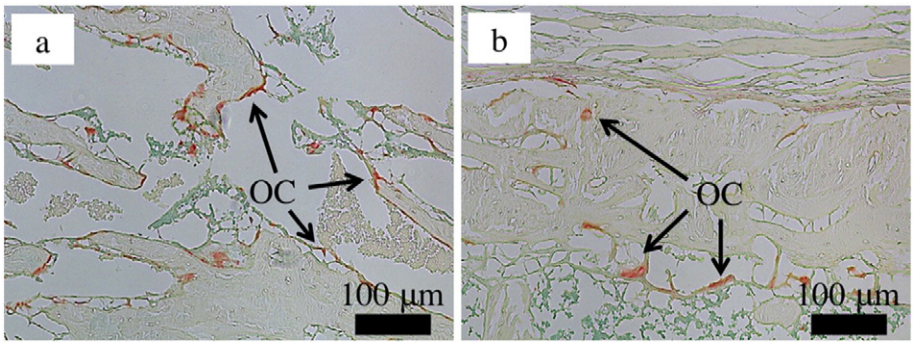

Fig. 9. TRAP stained samples (Mg-3w) showing the occurrence and location of osteoclasts (OCs) around cavities (a, 10×) and in the cortical region, on the endosteal and periosteal surfaces (b, 10×).

environment [31], diffuses through the tissues and is eliminated by the blood flow and renal system [32]. If diffusion is slower than the gas production, gas will accumulate in tissue cavities. The absence of voids at 6w suggest that degradation slowed to allow for complete gas absorption by this time. Similar results have been observed in previous studies on Mg alloys [13,32–34].

The thermodynamic predictions along with previous work in the field suggest that the layer forming on Mg alloys is $Mg(OH)_2$ [30,35]. For the pins in the current study, it can be hypothesized that the Mg is potentially substituted with small amounts of Ca and Sr. $Mg(OH)_2$ is considered safe in the body and has been suggested to comprise the osteoconductive properties observed of Mg [36]. The $Mg(OH)_2$ will react to form soluble $MgCl_2$, but its presence could be stabilized by local accumulation of Mg-Ca phosphates [30,34]. The amount of Mg and Ca released from the implant is considered safe [37]. While the Sr content in the tissue was not measured, the amount of Sr released from the pin, even in the event of a burst release, is much smaller than the clinical therapeutic dose for Sr ranelate (5–20 mg per kilo per day) [38].

Bone tissue mineral density appears to increase with time. Since new bone is forming as the pin degrades, an increase in mineral density value with time confirms mineralization of the new tissue. It is expected that the mineral density is highest at the final time point, as the tissue had longer time to heal. Large scatter in the data at 1w and 3w is attributed to differences between animals, which are amplified at earlier time points due to trauma from pin insertion and differences in pin degradation.

Histology revealed few inflammatory cells and mild fibrosis, as seen at the early time points. This is expected post-surgery for an inert biomaterial and can be a sign of implant integration [39]. The few accumulations of inflammatory cells that were observed around the alloy pins were located around tissue cavities associated with gas formation, making the inflammatory cells more prevalent at the 1w and 3w time points. Bone resident cell infiltration was observed around all alloy implants while the PLLA was surrounded by fibrous tissue. The fibrous layer separating the bone and implant can be undesirable as it may jeopardize implant stability, which can lead to fixation failure [5,39] and also prevent further implant degradation.

Osteoclast activity represents bone remodeling, which is naturally occurring in bone tissue, but can also be an implication of implant separation [40]. Osteoclasts were primarily located in the cortical region and around tissue cavities. It is unclear if this trend is related to damage and consecutive bone remodeling resulting from drilling and pin insertion or a response to gas generation, or a combination of factors.

Table 1
Area fraction of the tissue that is occupied by osteoclasts at the different time points.

	Mg-1w	Mg-3w	Mg-6w	PLLA-6w	Ctrl-6w
Osteoclast area (%)	0.51 ± 0.37	0.90 ± 0.49	0.11 ± 0.08	0.59 ± 0.40	0.05 ± 0.07

The current study investigates the *in vivo* response to the as-cast Mg–1.0 wt.%Ca–0.5 wt.%Sr alloy, with promising results. It is worth noting, that properties of the material, such as degradation rate, can be tailored by processing, alloying, coatings *etc*. [16,41,42], which may be relevant for future studies towards clinical applications. In addition to controlled degradation and biocompatibility, adequate strength of the material is important clinically, to avoid failure of the implant. One of the pins in the current study was found fractured upon dissection. Unfortunately the time of fracture is unknown, however it was still used in the data analysis. The alloy's strength has been reported elsewhere [16] by the authors.

5. Conclusions

This paper examines the *in vivo* local tissue response to a Mg–1.0 wt.%Ca–0.5 wt.%Sr alloy for degradable implant orthopedic applications. Despite early gas formation, the rat and local tissue responded reasonably well to the alloy implant with only a mild inflammatory response. Cell infiltration was observed around the degrading implant, with new bone replacing the implant as it degrades, with no histological evidence of fibrous encapsulation. In addition, mineralized bone was seen in the cortical region after 6w, with regained bone mineral density. On the contrary, PLLA biodegradable pins were intact at the end of the study period and were surrounded by fibrous tissue of varying thickness. Overall, there was minimal adverse host reaction, although an increased osteoclast activity around implants was observed at the early stages, which was attributed to tissue healing and bone remodeling. While alloy biocompatibility in the rat was confirmed, the effect of applied stress on the degradation behavior, and its resultant effect on bone remodeling and strength has yet to be specifically investigated. Relevant future investigations also include degradation studies determining the effect of implant morphology and location in the body.

Acknowledgments

The authors would like to acknowledge the undergraduate team at the University of Florida (UF), including Emily Hester, Daniella van der Merwe, Felix Chan, Kollin Kerr and Michael McGrath, as well as Dr. James Schumacher for their work in organizing the animal study. Tyrone Hutchinson and Dr. Michael W. Moser are recognized for their collaborative efforts and fruitful discussions. The work was supported by a grant from the University of Florida Office of Technology Licensing commercialization fund.

References

[1] J. Walker, S. Shadanbaz, T.B. Woodfield, M.P. Staiger, G.J. Dias, Magnesium biomaterials for orthopedic application: a review from a biological perspective, J. Biomed. Mater. Res. B Appl. Biomater. 102 (2014) 1316–1331.
[2] R.J. Narayan, Materials for medical devices, ASM Handbook, ASM International, 2012.

[3] O. Bostman, H. Pihlajamaki, Routine implant removal after fracture surgery: a potentially reducible consumer of hospital resources in trauma units, J. Trauma 41 (1996) 846–849.
[4] J.J. Jacobs, J.L. Gilbert, R.M. Urban, Corrosion of metal orthopaedic implants, J. Bone Joint Surg. Am. 80 (1998) 268–282.
[5] K. Modjarrad, S. Ebnesajjad, Handbook of Polymer Applications in Medicine and Medical Devices, Elsevier, United States, 2014.
[6] O.M. Bostman, Osteolytic changes accompanying degradation of absorbable fracture fixation implants, J. Bone Joint Surg. (Br.) 73 (1991) 679–682.
[7] N.J. Hallab, J.J. Jacobs, Biologic effects of implant debris, Bull. NYU Hosp. Jt. Dis. 67 (2009) 182–188.
[8] A.R. Amini, J.S. Wallace, S.P. Nukavarapu, Short-term and long-term effects of orthopedic biodegradable implants, J. Long-Term Eff. Med. Implants 21 (2011) 93–122.
[9] M. Walton, N.J. Cotton, Long-term in vivo degradation of poly-L-lactide (PLLA) in bone, J. Biomater. Appl. 21 (2007) 395–411.
[10] M.M. Avedesian, H. Baker, ASM International, Handbook committee, Magnesium and Magnesium Alloys, Materials Park, OH, ASM International, 1999.
[11] J.P. Paul, Strength requirements for internal and external prostheses, J. Biomech. 32 (1999) 381–393.
[12] H. Hornberger, S. Virtanen, A. Boccaccini, Biomedical coatings on magnesium alloys — a review, Acta Biomater. 8 (2012) 2442–2455.
[13] Z.J. Li, X.N. Gu, S.Q. Lou, Y.F. Zheng, The development of binary Mg–Ca alloys for use as biodegradable materials within bone, Biomaterials 29 (2008) 1329–1344.
[14] J.Y. Jung, S.J. Kwon, H.S. Han, J.Y. Lee, J.P. Ahn, S.J. Yang, et al., In vivo corrosion mechanism by elemental interdiffusion of biodegradable Mg–Ca alloy, J. Biomed. Mater. Res. B Appl. Biomater. 100B (2012) 2251–2260.
[15] H.S. Han, Y.Y. Kim, Y.C. Kim, S.Y. Cho, P.R. Cha, H.K. Seok, et al., Bone formation within the vicinity of biodegradable magnesium alloy implant in a rat femur model, Met. Mater. Int. 18 (2012) 243–247.
[16] I.S. Berglund, H.S. Brar, N. Dolgova, A.P. Acharya, B.G. Keselowsky, M. Sarntinoranont, et al., Synthesis and characterization of Mg–Ca–Sr alloys for biodegradable orthopedic implant applications, J. Biomed. Mater. Res. B Appl. Biomater. 100 (2012) 1524–1534.
[17] M. Bornapour, M. Celikin, M. Cerruti, M. Pekguleryuz, Magnesium implant alloy with low levels of strontium and calcium: the third element effect and phase selection improve bio-corrosion resistance and mechanical performance, Mater. Sci. Eng. C Mater. Biol. Appl. 35 (2014) 267–282.
[18] H.S. Brar, J. Wong, M.V. Manuel, Investigation of the mechanical and degradation properties of Mg–Sr and Mg–Zn–Sr alloys for use as potential biodegradable implant materials, J. Mech. Behav. Biomed. Mater. 7 (2012) 87–95.
[19] P.J. Marie, Strontium ranelate: a physiological approach for optimizing bone formation and resorption, Bone 38 (2006) 10–14.
[20] L. Maimoun, T.C. Brennan, I. Badoud, V. Dubois-Ferriere, R. Rizzoli, P. Ammann, Strontium ranelate improves implant osseointegration, Bone 46 (2010) 1436–1441.
[21] E. Bonnelye, A. Chabadel, F. Saltel, P. Jurdic, Dual effect of strontium ranelate: stimulation of osteoblast differentiation and inhibition of osteoclast formation and resorption in vitro, Bone 42 (2008) 129–138.
[22] O.Z. Andersen, V. Offermanns, M. Sillassen, K.P. Almtoft, I.H. Andersen, S. Sørensen, et al., Accelerated bone ingrowth by local delivery of strontium from surface functionalized titanium implants, Biomaterials 34 (2013) 5883–5890.
[23] J. Yan, J.F. Sun, P.K. Chu, Y. Han, Y.M. Zhang, Bone integration capability of a series of strontium-containing hydroxyapatite coatings formed by micro-arc oxidation, J. Biomed. Mater. Res. A 101 (2013) 2465–2480.
[24] X. Lin, X. Yang, L. Tan, M. Li, X. Wang, Y. Zhang, et al., In vitro degradation and biocompatibility of a strontium-containing micro-arc oxidation coating on the biodegradable ZK60 magnesium alloy, Appl. Surf. Sci. 288 (2014) 718–726.
[25] D.L. Hickman, M. Swan, Use of a body condition score technique to assess health status in a rat model of polycystic kidney disease, J. Am. Assoc. Lab. Anim. Sci. 49 (2010) 155–159.
[26] T. Kraus, S.F. Fischerauer, A.C. Hanzi, P.J. Uggowitzer, J.F. Loffler, A.M. Weinberg, Magnesium alloys for temporary implants in osteosynthesis: in vivo studies of their degradation and interaction with bone, Acta Biomater. 8 (2012) 1230–1238.
[27] N. Erdmann, N. Angrisani, J. Reifenrath, A. Lucas, F. Thorey, D. Bormann, et al., Biomechanical testing and degradation analysis of MgCa0.8 alloy screws: a comparative in vivo study in rabbits, Acta Biomater. 7 (2011) 1421–1428.
[28] L. Xu, G. Yu, E. Zhang, F. Pan, K. Yang, In vivo corrosion behavior of Mg–Mn–Zn alloy for bone implant application, J. Biomed. Mater. Res. A 83 (2007) 703–711.
[29] M. Pourbaix, Atlas of Electrochemical Equilibria in Aqueous Solutions, Pergamon Press Ltd., Bristol, 1966.
[30] G. Song, Corrosion of Magnesium Alloys, Woodhead Publishing Limited, Cambridge, 2011.
[31] J. Kuhlmann, I. Bartsch, E. Willbold, S. Schuchardt, O. Holz, N. Hort, et al., Fast escape of hydrogen from gas cavities around corroding magnesium implants, Acta Biomater. 9 (2013) 8714–8721.
[32] F. Witte, N. Hort, C. Vogt, S. Cohen, K.U. Kainer, R. Willumeit, et al., Degradable biomaterials based on magnesium corrosion, Curr. Opin. Solid State Mater. Sci. 12 (2008) 63–72.
[33] S.F. Fischerauer, T. Kraus, X. Wu, S. Tangl, E. Sorantin, A.C. Hänzi, et al., In vivo degradation performance of micro-arc-oxidized magnesium implants: a micro-CT study in rats, Acta Biomater. 9 (2013) 5411–5420.
[34] F. Witte, V. Kaese, H. Haferkamp, E. Switzer, A. Meyer-Lindenberg, C.J. Wirth, et al., In vivo corrosion of four magnesium alloys and the associated bone response, Biomaterials 26 (2005) 3557–3563.
[35] B.A. Shaw, Corrosion of magnesium and magnesium-base alloys, in: S.D. Cramer, B.S. Covino Jr. (Eds.), ASM Handbook, ASM International, Materials Park, OH 2003, pp. 692–696.
[36] C. Janning, E. Willbold, C. Vogt, J. Nellesen, A. Meyer-Lindenberg, H. Windhagen, et al., Magnesium hydroxide temporarily enhancing osteoblast activity and decreasing the osteoclast number in peri-implant bone remodelling, Acta Biomater. 6 (2010) 1861–1868.
[37] B. Venugopal, T.D. Luckey, Metal Toxicity in Mammals, Plenum Press, New York, 1978.
[38] P.J. Meunier, D.O. Slosman, P.D. Delmas, J.L. Sebert, M.L. Brandi, C. Albanese, et al., Strontium ranelate: dose-dependent effects in established postmenopausal vertebral osteoporosis—a 2-year randomized placebo controlled trial, J. Clin. Endocrinol. Metab. 87 (2002) 2060–2066.
[39] J.M. Anderson, A. Rodriguez, D.T. Chang, Foreign body reaction to biomaterials, Semin. Immunol. 20 (2008) 86–100.
[40] E.M. Greenfield, Y. Bi, A.A. Ragab, V.M. Goldberg, R.R. Van De Motter, The role of osteoclast differentiation in aseptic loosening, J. Orthop. Res. 20 (2002) 1–8.
[41] I.S. Berglund, B. Mobley, M.A. Wener, H.B. Henderson, M.V. Manuel, The effect of hot rolling on the microstructure and degradation behaviour of a Mg–Ca–Sr alloy, Eur. Cell Mater. 28 (2014).
[42] H.S. Brar, J.P. Ball, I.S. Berglund, J.B. Allen, M.V. Manuel, A study of a biodegradable Mg–3Sc–3Y alloy and the effect of self-passivation on the in vitro degradation, Acta Biomater. 9 (2013) 5331–5340.